Applied Surface Science 539 (2021) 148232

Contents lists available at ScienceDirect

Applied Surface Science

journal homepage: www.elsevier.com/locate/apsusc

Microfluidic-integrated graphene optical sensors for real-time and ultra-low flow velocity detection

Tiange Wu [a,1], Junfeng Shen [b,1], Zongwen Li [a,1], Fei Xing [a,*], Wei Xin [c], Zhao Wang [a], Guowei Liu [a], Xue Han [a], Zhongsheng Man [a], Shenggui Fu [a,*]

[a] School of Physics and Optoelectronic Engineering, Shandong University of Technology, Zibo 255049, China
[b] School of Physical Science and Technology, Southwest Jiaotong University, Sichuan 614202, China
[c] The Guo China-US Photonics Laboratory, State Key Laboratory of Applied Optics, Changchun Institute of Optics, Fine Mechanics, and Physics, Chinese Academy of Sciences, Changchun, China

ARTICLE INFO

Keywords:
Microfluidics
Graphene optical sensors
Polarization-dependent effect
Flow velocity

ABSTRACT

As microfluidic technology continues to mature, many techniques are being developed to monitor the flow of microfluidics. However, achieving breakthroughs in the real-time detection of ultra-low flow velocity and non-conductive liquid in microfluidic environments remains a major challenge. Here, microfluidic-integrated graphene optical sensorswith a sensitivity of 4.65×10^5 mV·s·m^{-1} and a detection limit of 4.9×10^{-5} m·s^{-1} were designed to address these challenges. We reported our efforts to quantify the impact of ultra-low flow velocity driven by ultra-small levels of pressure. A flow velocity of 3.7×10^{-4} m·s^{-1} was detected with a signal-to-noise ratio of approximately 7.5. A high-quality graphene layer that was directly grown on glass by an improved low-pressure chemical vapor deposition method and provided several advantages, including controllable thickness, high uniformity, high stability, and corrosion resistance. Graphene also has an excellent polarization-dependent effect. It was extremely sensitive to pressure-driven microfluidic flow because of the interaction between polarization light and the quartz glass/graphene film/medium multilayer-coupling structure, which fed back the signals in real-time. This novel sensor represents a breakthrough in the ultra-low level detection of the flow velocity of non-conductive microfluidics. We expect this sensor to have a broad array of applications in the field of microfluid velocity measurement.

1. Introduction

Microfluidic-integrated sensors have rapidly evolved over the years and have diverse applications in physics analysis [1–3], chemical analysis [4], biological analysis [5,6], and even other fields, such as biomedicine [4–7]. The booming development of microfluidic chips has made the need to measure microfluidic flow velocity more pressing, especially for the accurate detection of ultra-low flow velocity in real-time. Microfluidic chips are characterized by their small size and working space. The performance of fluids under microscale and with microstructure is different from that of traditional macroscopic fluids. The most noteworthy differences that need to be taken into account are the size [8,9] as well as capillary and laminar flow [10,11]. Extensive work has been devoted to examining measurements of fluid flow. A flow velocity measuring instrument based on the ultrasonic Doppler effect was proposed as early as in the 1980s and 1990s [12,13]. By adding tracer particles to the liquid to be tested (tracer particles cannot react with the liquid to be measured), the frequency at which the ultrasonic waves are generated before and after the reflection (acting on the tracer particles) can be captured and the frequency difference calculated. The flow velocity of the traced particles in the fluid can then be used to simulate that of the liquid being measured. In recent years, much progress has been made in the use of light-based Doppler correlation spectroscopy [1,14,15]. However, considering the non-polluting,

Abbreviations: MGOS, microfluidic-integrated graphene optical sensors; CVD, chemical vapor deposition; LPCVD, low-pressure chemical vapor deposition; AFM, atomic force microscope; SEM, scanning electron microscope; XPS, X-ray photoelectron spectroscopy; OP, ordinary-pressure; LP, low-pressure; PDMS, polydimethylsiloxane; ECG, electrocardiogram.

* Corresponding authors.
E-mail addresses: xingfei@sdut.edu.cn (F. Xing), fushenggui@sdut.edu.cn (S. Fu).

[1] These authors equally contributed to this work.

https://doi.org/10.1016/j.apsusc.2020.148232
Received 3 July 2020; Received in revised form 16 October 2020; Accepted 19 October 2020
Available online 22 October 2020

accurate and real-time performance of microfluidic flow measurement, many obstacles still need to be overcome, including the inability to accurately monitor flow velocity in real-time, the complicated nature of experimental operations, and the introduction of other tracer substances.

Shankar Ghosh et al. [16] and Mainak Majumder et al. [17] made early attempts to solve these problems using the superhydrophobic properties and electrical properties of carbon nanotubes to achieve a wide range of flow velocity measurements of conductive liquid. However, the process of preparing a single carbon nanotube microfluidic sensor is extremely complicated, and the repeatability of device preparation is difficult to control, which limits the applicability of this technology. Graphene, with a special lattice and electronic structure, exhibits excellent physical properties in the fields of electronics and optics [18–22]. In 2012, a novel graphene-based field-effect transistor was used to measure microfluidic flow velocity to characterize the relationship between potential and flow velocity by measuring information related to the flow potential in the microfluidic channel [23]. Using the excellent two-dimensional structural and electrical properties of graphene, this sensor permitted simple and real-time flow velocity measurements to be taken without tracking and had an ultra-high sensitivity with a detection limit of 10^{-3} m·s^{-1}. However, this type of sensor is limited by the stringent requirements and dependencies of the conductivity of the fluids being tested. In 2020, Savina et al. has worked on the topic of the flow velocity of two-phase slug flow in microfluidic channels [24]. They designed the low-cost and non-invasive portable system to realize real-time monitoring of the state of two immiscible fluids in the microfluidic channel, and the flow velocity range of 0∼0.2 m/s was monitored. The monitoring system cannot accurately measure ultra-low level flow velocity. In addition, it has obvious limitations on the liquid that can be sensed. Moreover, the temporal and spatial resolutions of the electrical sensors are greatly restricted relative to those of optical sensing. Thus, microfluidic-integrated graphene optical sensors (MGOS) provide extremely useful real-time and ultra-low flow velocity detection platforms for liquid flow, even blood.

In addition to its excellent electrical properties, graphene also exhibits excellent optical properties, especially its interaction properties with light [25]. Over the past several years, graphene-based optical sensors have played a major role in real-time, unlabeled, and sensitive sensing and have great potential to be applied as a novel sensor [26,27]. Here, we proposed that the optical properties of graphene could be used to tentatively detect the ultra-low flow velocity of micron per second levels in microfluidic chips. Flow velocity measurement is a dynamic measurement process. In order to achieve ultra-low-level dynamic measurement of flow velocity, it hold out high requirments to the quality of graphene, the coupling between graphene and optical system, the workmanship of microfluidic channel, and the control of the measurement process. To make this possible, overall innovation at the scientific research level is required, the preparation of high-quality graphene-based optical chips, sophisticated system design and complete signal analysis are essential. In this paper, the low-pressure chemical vapor deposition (LPCVD) method is utilized to rapidly grow graphene directly on a glass substrate without transferring which can avoid pollution and damage, and maintain the excellent photoelectric properties of graphene film. Real-time and ultra-sensitive signal feedback can be realized through graphene's excellent polarization-dependent effect. Based on this, the flow velocity sensor has the potential to be used in the medical field for blood flow measurement such as measuring the blood flow velocity in coronary artery stenosis [28,29]. The technology may be of great help to the monitoring of critically ill patients.

2. Materials and methods

The chemical vapor deposition (CVD) method for growing graphene is relatively low-cost and compatible with the chip fabrication process [21,30,31]. Here, using an improved LPCVD method, we stimulated the growth of graphene films onto glass directly with the growth pressure below 300 Pa. In our research, we have managed to grow the graphene with a rapid and low-cost method so that it has both highly uniform and thickness-controlled properties [32]. Fig. 1 shows the image of atomic force microscope (AFM, Veeco, Dimension3100 microscope) and high resolution scanning electron microscope (SEM, America, FEI microscope) of graphene flim. The left side of Fig. 1A (AFM image) is the graphene film grown on a glass substrate, and the right side is the bare glass. It can be known from Fig. 1B that the thickness of the graphene film is 8.27 nm (∼24 layers). Surface roughness is an important parameter to characterize film flatness. The smaller the surface roughness is, the smoother the surface is. We provide you with an enlarged AFM image of the local region of graphene in Fig. 1C, the surface roughness of 8.27 nm graphene is 3.02 nm inside the box which indicates the whole surface graphene film is uniform. Fig. 1D shows the SEM image of the graphene film, which proves that the graphene film has almost no wrinkle (the characterization results FigureS1 in the Supplementary Materials also shows the smooth and low defect advantages of graphene grown by the LPCVD method).

Furthermore, we verified the advantages of the improved LPCVD method for growing graphene films. We obtained the Raman spectrum of the graphene film (Horiba, LabRAMHREvolution) as shown in Fig. 2A. The D peak is located at 1332.3 cm^{-1} and the G peak at 1562.9 cm^{-1}, the 2D peak is located at 2672.9 cm^{-1} [33]. The calculated I_D/I_G is 0.94, which indicates that graphene has a lower defect level. The samples were also subjected to X-ray photoelectron spectroscopy (XPS) at 1486.6 eV and 400 W to describe the characteristics of graphene films. The characteristics of graphene films grown by ordinary- pressure (OP) CVD and LPCVD methods were measured by XPS, as shown in Fig. 2B. The results highlighted the C1s peak (284.8 eV) and the O1s peak (532.7 eV). Compared with the OPCVD graphene film, the O atom concentration of the LPCVD graphene film is 8.42%, which is reduced by 35.9%. In which, it shows that the LPCVD process significantly reduces the level of covalently bonded oxygen functional groups, yet still a few oxygen-containing functional groups exist. To further analyze the composition of the carbon region, high-resolution narrow scans of the carbon region from LPCVD and OPCVD graphene films are shown in Fig. 2C and D. OPCVD graphene films showed significant peaks of 284.2 eV (C═C), 285 eV (C-C), 286.4 eV (C-O), 287.8 eV (C═O), while LPCVD graphene films only showed significant peaks of 284.2 eV (C═C), 285 eV (C-C), 286.4 eV (C-O), and almost negligible peaks of 287.8 eV (C═O). Therefore, we conclude that LPCVD graphene films have lower oxygen content and can exhibit better electro-optical properties, which is the ideal graphene-based optical sensor chip. This procedure meets both sensitive sensing of the graphene layer and optical transparency requirements. By using this high-performance graphene glass, we devised the "quartz glass/graphene film/liquid (water, blood or other liquid)" multilayer film structure under reflection-coupling conditions. Under reflection-coupling conditions, the graphene layer exhibits excellent polarization dependence [34]: that is, the transverse-electric (TE) mode after passing through the graphene film is mostly absorbed by graphene, whereas the transverse-magnetic (TM) mode hardly absorbs. To examine this effect, we set up an ultra-sensitive, real-time MGOS system without tracer and liquid conductivity requirements. Consideration of the uneven distribution in flow velocity in the microfluidic channel as a result of the maldistribution of the pressure is essential. In addition, the viscous resistance, which is generated between the walls of the microfluidic channels and the liquid, also affects the flow velocity in the microfluidic channels [35]. Here, graphene-based sensors combined with spatial light field modulation make their temporal and spatial resolution unrestricted, and the flow velocity in the microfluidic channel is sensed by amplifying the target signal in real-time. Thus, the highly sensitive flow sensing is expected to apply to biomedical sensors.

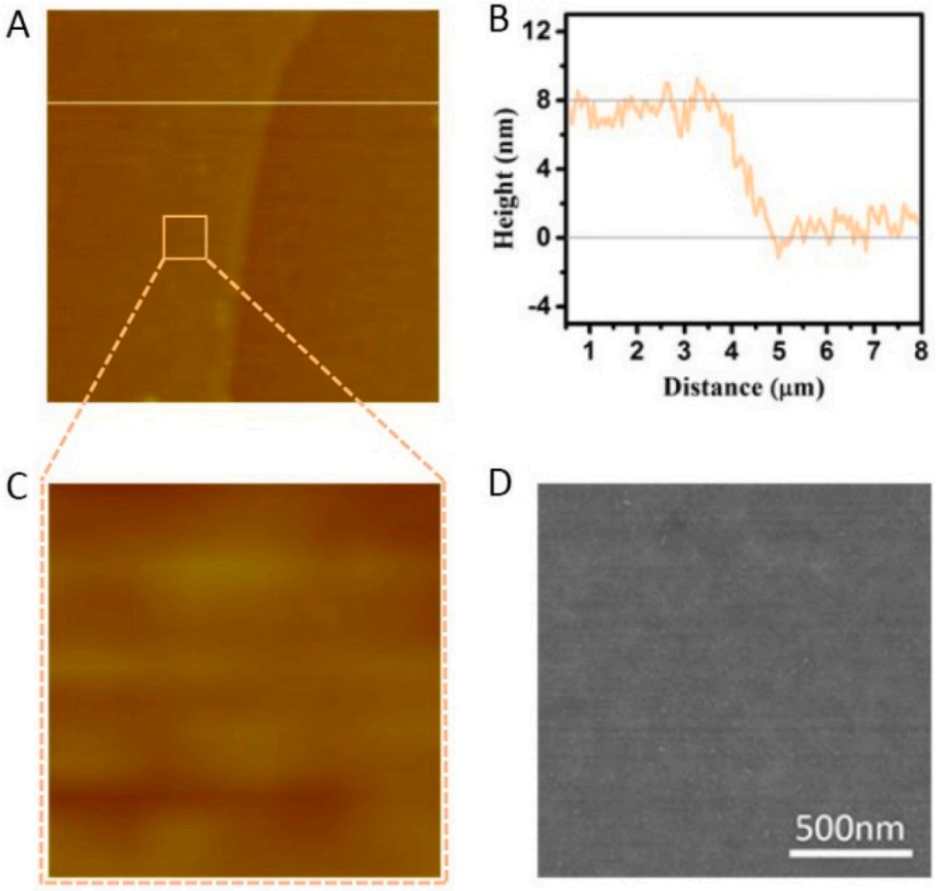

Fig. 1. (A) AFM image of graphene film grown by LPCVD. (B) The height of graphene film. (C) Locally enlarged image of graphene AFM image. (D) SEM image of graphene film grown by LPCVD.

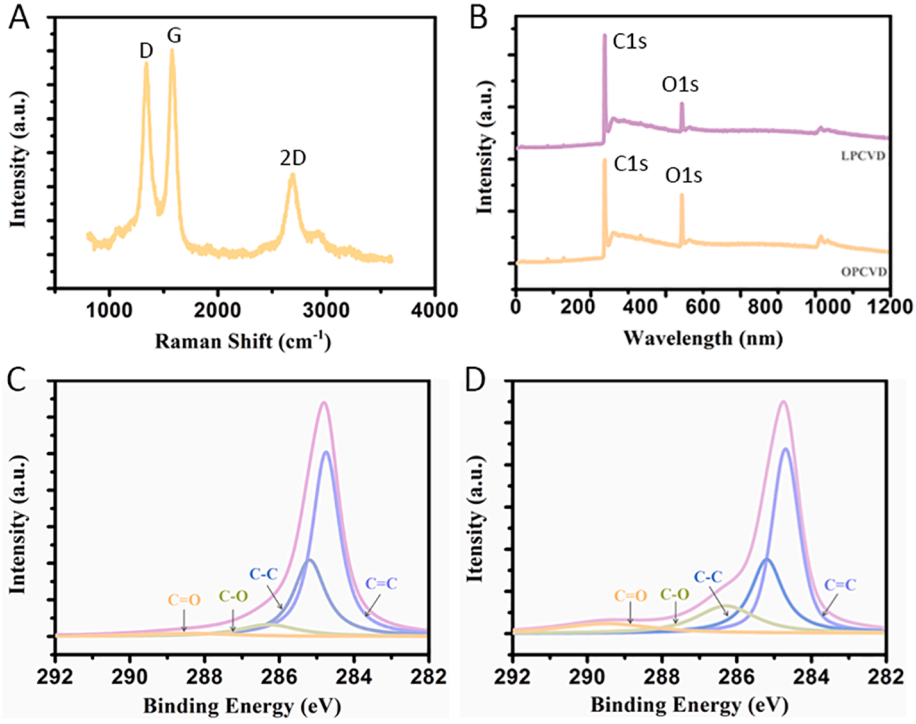

Fig. 2. (A) Raman spectra of graphene film grown by LPCVD. (B) Comparison of XPS spectra of graphene film grown by LPCVD and OPCVD methods. (C-D) The high-resolution narrow scans of the carbon region from LPCVD and OPCVD graphene film.

3. Theoretical analysis of MGOS

In Fig. 3A, we established a theoretical model of a graphene-based flow sensor. Through the multilayer film coupling structure (the graphene is sandwiched at the interface of medium 1 (n_1) and medium2 (n_2)) of the high refractive index medium (quartz glass, $n_1 = 1.47$)/ graphene film ($n_G = 2.73 + 1.35i$) [36] and low refractive index medium (deionized water, $n_2 = 1.33$), a portion of the energy can pass through the interface between medium 1 and medium 2 and finally propagate along the interface. The enhancing effect of light interaction with graphene is achieved in the critical state of total reflection.

Fig. 3B simulates the reflectance difference between TE mode and TM mode at different thicknesses. According to the results of the simulation, we chose a He-Ne laser with an incident wavelength of 632.8 nm and selected a graphene film with a thickness of 8.27 nm to obtain the best amplification and high sensitivity. Moreover, we have elaborately simulated the reflectivity of graphene with different thicknesses under different incident angles of TE and TM modes, as shown in Fig. 3C-E. The reflectivity experiment of the TM and TE modes after passing the graphene layer was carried out. The experimental results (see Supplementary Materials FigureS2) also confirmed that the 8.27 nm graphene film is an ideal choice. This polarization-dependent absorption of graphene is sensitive to changes in the wavelength of the incident light, the thickness of the graphene, and the refractive index of medium 2. Thus, we suggest that the coupling structure based on graphene film is sensitive to changes in the refractive index caused by external conditions.

4. Experimental setup

As shown in Fig. 4, the experiment was configured with a He-Ne linearly polarized laser with a light source of 632.8 nm, which then passed through an attenuator, a polarizer, and a quarter-wave plate separately, obtaining stable, power-adjustable circularly polarized light. The light spot with a lateral size of 1.13 mm^2 (the radius was approximately 0.6 mm) was formed on the quartz glass/graphene film/liquid multilayer film coupling structure, which is much smaller than the size of the microchamber ($6 \times 4 \times 0.05$ mm^3). Next, the beam passed through the Wollaston prism, and the circularly polarized light reflected from the multilayer film coupling structure was separated into TE and TM modes having the same optical path. By the two beams of light having the same optical path, common-mode noise can be significantly suppressed, and relatively stable experimental results can be obtained [37]. The two beams of light then entered the detection hole of the balanced detector, thereby converting the optical signal into an electrical signal.

5. Results and discussion

We found that the refractive index varied with the liquid flow velocity. This pattern likely stemmed from the fact that the flow velocity varied with the pressure difference between the inlet and the outlet. When this pressure difference increases, the liquid becomes increasingly compressed, and the refractive index of the liquid increases. The relationship between the *RI* change (*dn*) and pressure (*P*) of ultrasonic in water was reported as [38]:

$$\frac{dn}{dP} = 1.35 \times 10^{-10} \tag{1}$$

The interaction of the multilayer film-coupling structure based on the graphene film with light produced a significant response to the change in the refractive index (this part of the theory is addressed in the Supplementary Materials). Thus, physical parameters, such as flow velocity, pressure, refractive index and voltage, are associated. In the following, we consider the liquids sensed by the sensing system to have different flow velocities and corresponding voltages. During the experiment, the pressure was controlled by the flow velocity control valve, and it is guaranteed that there was only one variable pressure during this process to accurately measure the voltage signal caused by the pressure difference or the flow velocity. We therefore defined sensitivity *S* and detection limits *D*. The sensitivity *S* is the ratio of unit voltage to unit flow velocity. The detection limit *D* can be described as the minimum flow velocity that can be detected:

$$S = dU/dv \tag{2}$$

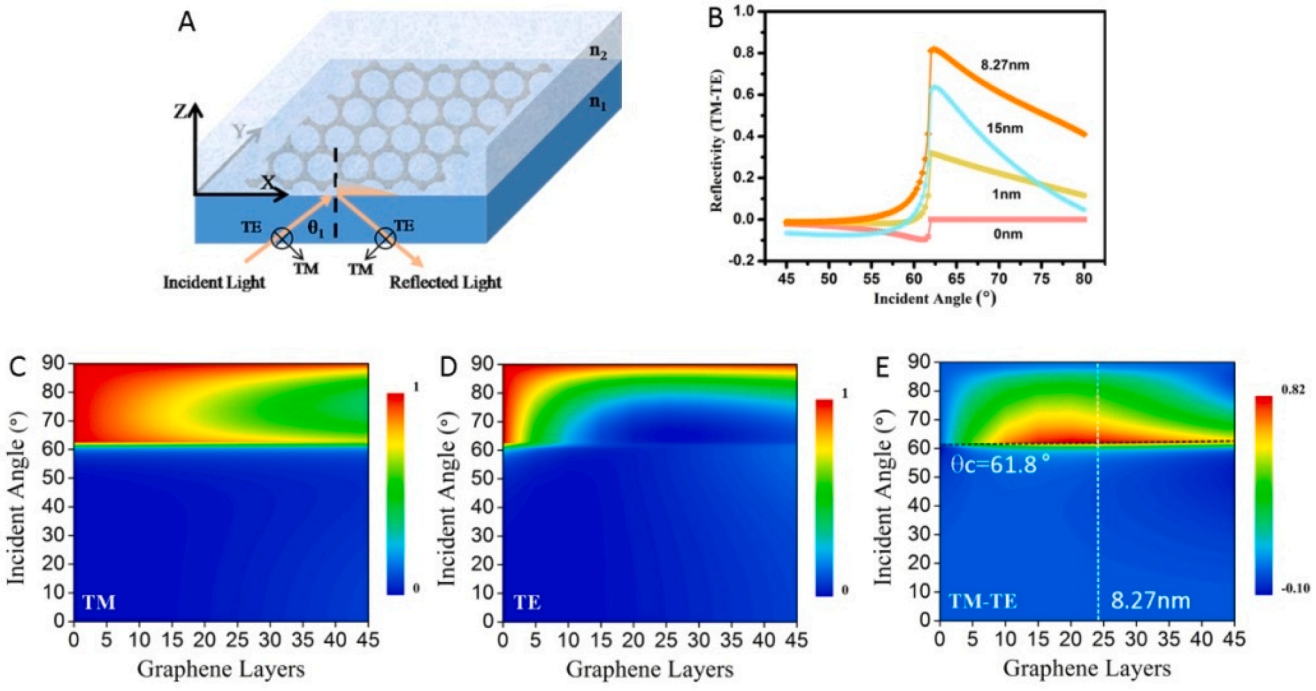

Fig. 3. (A) The theoretical model of a graphene-based flow velocity sensor. (B) Simulation of the difference in absorption of TM-TE at different thicknesses of graphene. (C-E) The different reflectances (the incident wavelength is 632.8 nm) exhibited by the TE mode, TM mode, and TM-TE under reflective conditions.

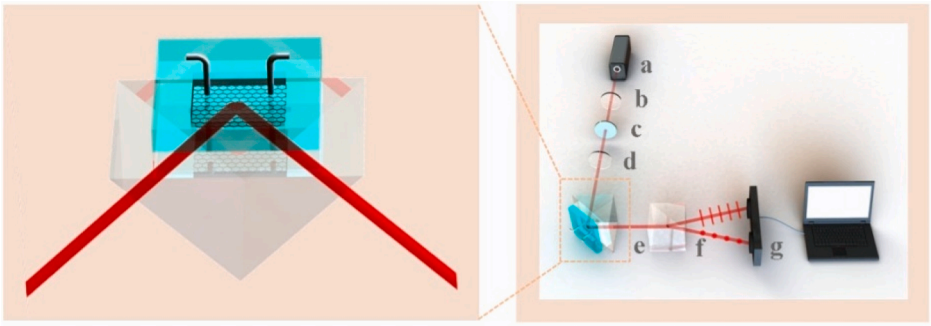

Fig. 4. Diagram of the experimental setup of the graphene-based microfluidic flow-sensing system. a: laser, b: attenuator, c: polarizer, d: $\lambda/4$ plate, e: Quartz glass/Graphene film/Medium multilayer coupling structure, f: Wollaston prism, g: balance detector.

$$D = N/S \tag{3}$$

where dU is the change in the voltage signal caused by the flow velocity (pressure difference), dv is the difference in the flow velocity of the sensing liquid (deionized water or other liquid) from the flowing state to the stationary state. Based on the experimental results, Fig. 5A presented the response of the voltage ($\triangle V = 150$ mV) when an ultra-small flow velocity ($v = 0.37$ mm/s) was detected. N is the noise signal, and a signal-to-noise ratio of approximately 7.5 was obtained by the calculation. To obtain moreaccurate experimental data, we established a three-dimensional model of the microfluidic channel, which had a size of $6 \times 4 \times 0.05$ mm^3, to calculate the pressure and flow velocity inside the microfluidic channel. Regarding the experimentally measured ultra-low flow velocity of 0.37 mm/s, Fig. 5B shows the pressure distribution image at this stable flow velocity (0.37 mm/s), and Fig. 5C shows the corresponding flow velocity distribution image. In the imaging figures, uniform flow velocity and pressure gradients were evident at 300 Pa and 10^{-4} m/s. According to the formula, the sensitivity and detection limit of the sensor can be calculated to be 4.65×10^5 mV·s·m^{-1} and 4.9×10^{-5} m·s^{-1} respectively.

The lab-on-a-chip device designed here yields the conditions of a reagent solution with a velocity at a magnitude that suggests laminar behavior. This prediction implies that the full momentum balance and continuity equations for reagent solution (treated here as incompressible flow (an incompressible fluid is not one that is incompressible under external forces or temperature etc., but one whose density changes with velocity are negligible [39])) could be solved based on the Navier-Stokes equations in the time domain:

$$\rho\frac{\partial u}{\partial t} - \nabla\cdot\mu(\nabla u + (\nabla u)^T) + \rho u\cdot\nabla u + \nabla P = 0 \tag{4}$$

$$\nabla\cdot u = 0 \tag{5}$$

where ρ denotes density (SI unit: kg/m^3), u denotes the velocity vector (SI unit: m·s^{-1}), μ denotes dynamic viscosity (SI unit: Pa·s), T denotes absolute temperature (SI unit: K), and p denotes pressure (SI unit: Pa).

The reagent solution here was deionized water, with its corresponding density and viscosity values. The geometry of the microfluidics chip and initial conditions were designed according to the experimental conditions. The corresponding pressure and velocity are provided for the inlet.

Deionized water was selected as the standard research object for the experiment. Fig. 6A is the reflectivity difference (TM-TE) simulation of several different refractive index media (water, NaCl solution with the concentration of 5%, and ethylene glycol) at the fixed incidence angle. When there was a slight difference in the refractive index of the liquid, the reflectivity difference (TM-TE) changed greatly. Moreover, the graphene film gained by the LPCVD method acquires hydrophobic properties, and the viscous force generated by the shearing action on the velocity isosurface is reduced, making a relatively stable diffusion process in the microfluidics system, which is advantageous for the sensor for obtaining information on relative accurate flow velocity. Furthermore, there were only a few free charges in the deionized water, which revealed that the sensing system has no limitation on the conductivity of the sensing liquid. For this reason, the infusion set was connected to the inlet of the microfluidic chip. By making the valve control switch to be in the "on" state, the voltage signal corresponding to the fluid in the flowing state was obtained. In contrast, when the valve control switch was closed, the corresponding voltage signal in the static state was obtained. The pressure varied depending on the position of the valve control switch, and Fig. 6B shows the relationship between the voltage signals and the different flow velocity signals at the ultra-low velocity level. Fig. 6C shows a robust linear relationship between flow velocity and voltage. More importantly, based on the experimental and simulation results, we have also discovered laminar and turbulent phenomena at the ultra-low flow velocity level of several mm/sin microfluidic chips with this novel sensing system. This phenomenon is presumed to be

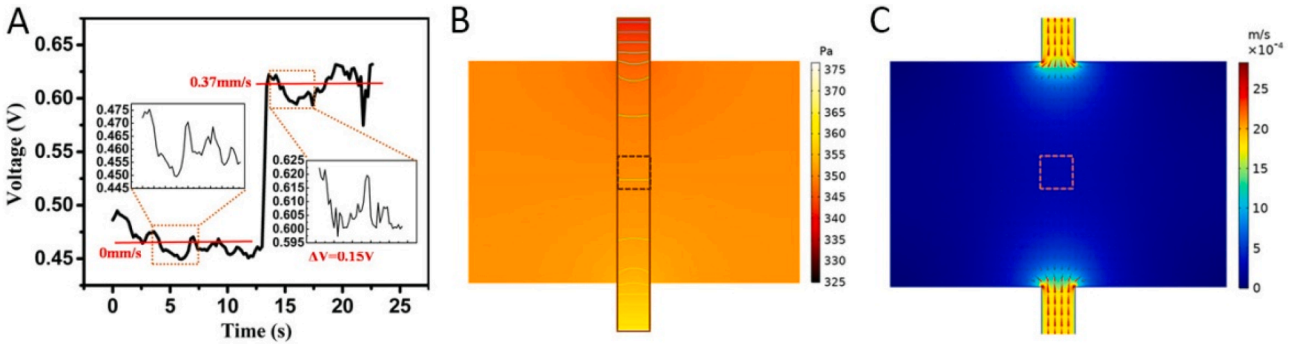

Fig. 5. (A) The response of the voltage when an ultra-small flow rate was detected. (B) The pressure distribution image at the flow rate of 0.37 mm/s. (C) The velocity distribution image at the flow rate of 0.37 mm/s.

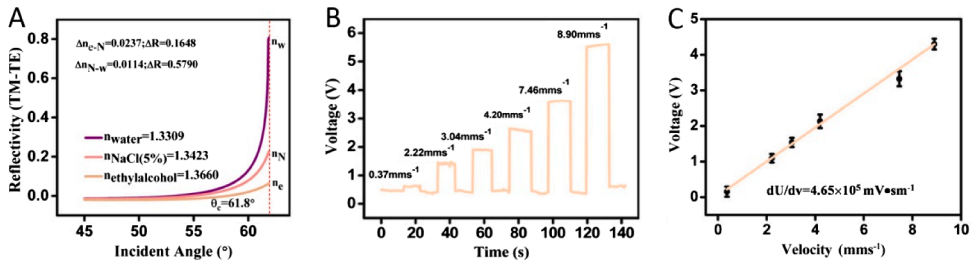

Fig. 6. (A) The reflectivity simulation of several different media (the three media were deionized water, NaCl solution at a concentration of 5% and ethyl alcohol). (B) The relationship between voltage signals (the value of the ordinate was the absolute value of the voltage) and the velocity level. (C) The linear relationship between the detected voltage signal (the value of the ordinate was the absolute value of the voltage) and the flow rate.

related not only to the pressure difference across the microfluidic channel but also to the size of the microfluidic channel.

In sum, we designed novel MGOS to enable accurate measurement of ultra-low flow velocity changes based on the direct growth of technology related to graphene glass and graphene multilayer film-coupling structure. The sensitivity and detection limit of the MGOS were 4.65 $\times$ 10^5 mV·s·m^{-1} and 4.9 $\times$ 10^{-5} m·s^{-1}, respectively, which are the highest levels reported to date. In addition to ultra-high sensitivity, this sensor also has the advantages of providing simple and real-time sensing without tracking, non-conductive liquid measurement, pollution-free measurement, and reliable, chip-integrated graphene. Moreover, the graphene-based sensor detected changes in ultra-low flow velocity with the spatial light field, and the temporal and spatial resolution can be easily implemented. The pressure and flow velocity in the microfluidics were also consistent under ultra-low flow velocity conditions. This finding provides a reliable technique for further study of the basic characteristics of trace fluids in ultra-low flow velocity stages. This tool will also be of great research significance in the analysis of ultra-low flow and micro-flow fluid environments.

CRediT authorship contribution statement

Tiange Wu: Data curation, Investigation, Methodology, Validation, Writing - original draft. **Junfeng Shen:** Formal analysis, Funding acquisition, Methodology, Software. **Zongwen Li:** Investigation, Methodology, Project administration, Resources. **Fei Xing:** Conceptualization, Formal analysis, Funding acquisition, Project administration, Writing - review & editing. **Wei Xin:** Funding acquisition, Formal analysis, Investigation. **Zhao Wang:** Software, Visualization. **Guowei Liu:** Data curation, Investigation. **Xue Han:** Data curation, Investigation. **Zhongsheng Man:** Funding acquisition, Supervision, Validation. **Shenggui Fu:** Formal analysis, Investigation, Supervision, Validation.

Declaration of Competing Interest

The authors declare that they have no known competing financial interests or personal relationships that could have appeared to influence the work reported in this paper.

Acknowledgements

This work was supported by the National Natural Science Foundation of China (Grant No. 11604182, 118043, 61505109), Natural Science Foundation of Shandong Province (Grant No. ZR2016AB05), Youth Innovative Talents Attracting and Cultivating Plan of Colleges and Universities in Shandong Province (21) and Ministry of Education Chunhui Plan Cooperation Research Project (10801X10096030).

Appendix A. Supplementary data

Supplementary data to this article can be found online at https://doi.org/10.1016/j.apsusc.2020.148232.

References

[1] R. Leitgeb, L.F. Schmetterer, M. Wojtkowski, C.K. Hitzenberger, M. Sticker, A.F. Fercher, Flow velocity measurements by frequency domain short coherence interferometry, in: Coherence Domain Optical Methods in Biomedical Science and Clinical Applications VI. International Society for Optics and Photonics, vol. 4619, 2002, pp. 16-21.
[2] S. Balslev, A.M. Jorgensen, B. Bilenberg, K.B. Mogensen, D. Snakenborg, O. Geschke, J.P. Kutter, A. Kristensen, Lab-on-a-chip with integrated optical transducers, Lab Chip 6 (2006) 213–217.
[3] W. Xin, T.G. Wu, T.T. Zou, Y. Wang, W.S. Jiang, F. Xing, J.J. Yang, C.L. Guo, Ultrasensitive optical detection of water pressure in microfluidics using smart reduced graphene oxide glass, Front. Chem. 7 (2019).
[4] D. Mark, S. Haeberle, G. Roth, F. Von Stetten, R.Zengerle,Microfluidic lab-on-a-chip platforms: requirements, characteristics and applications, in: Microfluidics based microsystems, Springer, Dordrecht, 2010, pp. 305-376.
[5] P.S. Dittrich, A. Manz, Lab-on-a-chip: microfluidics in drug discovery, Nat. Rev. Drug Discovery 5 (2006) 210.
[6] V. Srinivasan, V.K. Pamula, R.B. Fair, An integrated digital microfluidic lab-on-a-chip for clinical diagnostics on human physiological fluids, Lab Chip 4 (2004) 310–315.
[7] K. Choi, J.Y. Kim, J.H. Ahn, J.M. Choi, M. Im, Y.K. Choi, Integration of field effect transistor-based biosensors with a digital microfluidic device for a lab-on-a-chip application, Lab Chip 12 (2012) 1533–1539.
[8] M. Gad-el-Hak, The MEMS handbook, CRC Press, 2001.
[9] K. Nakada, M. Fujita, G. Dresselhaus, M.S. Dresselhaus, Edge state in graphene ribbons: nanometer size effect and edge shape dependence, Phys. Rev. B 54 (1996) 17954.
[10] V. Cristini, Y.C. Tan, Theory and numerical simulation of droplet dynamics in complex flows-a review, Lab Chip 4 (2004) 257–264.
[11] K. Liu, H.J. Ding, J. Liu, Y. Chen, X.Z. Zhao, Shape-controlled production of biodegradable calcium alginate gel microparticles using a novel microfluidic device, Langmuir 22 (2006) 9453–9457.
[12] H.A. Kontos, Validity of cerebral arterial blood flow calculations from velocity measurements, Stroke 20 (1989) 1–3.
[13] J.G. Santiago, S.T. Wereley, C.D. Meinhart, D.J. Beebe, R.J. Adrian, A particle image velocimetry system for microfluidics, Exp. Fluids 25 (1998) 316–319.
[14] J. Lauri, M. Wang, M. Kinnunen, R. Myllylä, Measurement of microfluidic flow velocity profile with two Doppler optical coherence tomography systems, in: Optical Diagnostics and Sensing VIII. International Society for Optics and Photonics, vol. 68630F, 2008.
[15] T.J. Arbour, J. Enderlein, Application of dual-focus fluorescence correlation spectroscopy to microfluidic flow-velocity measurement, Lab Chip 10 (2010) 1286–1292.
[16] S. Ghosh, A.K. Sood, N. Kumar, Carbon nanotube flow sensors, Science 299 (2003) 1042–1044.
[17] M. Majumder, N. Chopra, R. Andrews, B.J. Hinds, Nanoscale hydrodynamics: enhanced flow in carbon nanotubes, Nature 438 (2005) 44.
[18] F. Bonaccorso, Z. Sun, T. Hasan, A.C. Ferrari, Graphene photonics and optoelectronics, Nat. Photonics 4 (2010) 611.
[19] K.S. Kim, Y. Zhao, H. Jang, S.Y. Lee, J.M. Kim, K.S. Kim, J.H. Ahn, P. Kim, J. Y. Choi, B.H. Hong, Large-scale pattern growth of graphene films for stretchable transparent electrodes, Nature 457 (2009) 706.
[20] J.F. Wu, H.T. Wang, Z.W. Su, M.H. Zhang, X.D. Hu, Y.J. Wang, Z.A. Wang, B. Zhong, W.W. Zhou, J.P. Liu, S.G. Xing, Highly flexible and sensitive wearable e-skin based on graphite nanoplatelet and polyurethane nanocomposite films in mass industry production available, ACS Appl. Mater. Interfaces 9 (2017) 38745–38754.
[21] J.F. Wu, Z.Y. Ma, Z. Hao, J.T. Zhang, P.F. Sun, M.H. Zhang, Y.K. Liu, Y.S. Cheng, Y. Li, B. Zhong, T. Zhang, L. Xia, W. Yao, X.X. Huang, H.T. Wang, H.P. Liu, F. Yan, E.C. Hsu, G.Z. Xing, Sheath-core fiber strain sensors driven by in-situ crack and elastic effects in graphite nanoplate composites, ACS Appl. Nano Mater. 2 (2019) 750–759.
[22] Z.W. Li, W.F. Zhang, F. Xing, Graphene optical biosensors, Int. J. Mol. Sci. 20 (2019) 2461.

[23] R.X. He, P. Lin, Z.K. Liu, H.W. Zhu, X.Z. Zhao, H.L. Chan, F. Yan, Solution-gated graphene field effect transistors integrated in microfluidic systems and used for flow velocity detection, Nano Lett. 12 (2012) 1404–1409.
[24] S. Gagliano, G. Stella, M. Bucolo, Real-time detection of slug velocity in microchannels, Micromachines 11 (2020) 241.
[25] M. Engel, M. Steiner, A. Lombardo, A.C. Ferrari, H.V. Löhneysen, P. Avouris, R. Krupke, Light–matter interaction in a microcavity-controlled graphene transistor, Nat. Commun. 3 (2012) 906.
[26] F. Xing, Y. Yang, J.F. Shen, W.S. Jiang, Z.B. Liu, S.W. Zhu, X.C. Yuan, Ultra-high sensitivity, multi-parameter monitoring of dynamical gas parameters using a reduced graphene oxide microcavity, Sens. Actuators, B 235 (2016) 474–480.
[27] F. Xing, Z.B. Liu, Z.C. Deng, X.T. Kong, X.Q. Yan, X.D. Chen, Q. Ye, C.P. Zhang, Y. S. Chen, J.G. Tian, Sensitive real-time monitoring of refractive indexes using a novel graphene-based optical sensor, Sci. Rep. 2 (2012) 1–7.
[28] J. Keegan, D. Firmin, P. Gatehouse, D. Longmore, The application of breath hold phase velocity mapping techniques to the measurement of coronary artery blood flow velocity: phantom data and initial in vivo results, Magn. Reson. Med. (1994).
[29] A. Karimipour, D. Toghraie, L.A. Abdulkareem, A. Alizadeh, M. Zarringhalam, A. Karimipour, Roll of stenosis severity, artery radius and blood fluid behavior on the flow velocity in the arteries: application in biomedical engineering, Med. Hypotheses (2020).
[30] X.S. Li, W.W. Cai, J. An, S. Kim, D.X. Yang, R. Piner, A. Velamakanni, I. Jung, E. Tutuc, S.K. Banerjee, L. Colombo, R.S. Ruoff, Large-area synthesis of high-quality and uniform graphene films on copper foils, Science 324 (2009) 1312–1314.
[31] M. Taghioskoui, Trends in graphene research, Mater. Today 12 (2009) 34–37.
[32] X.D. Chen, Z.L. Chen, W.S. Jiang, C. Zhang, J.Y. Sun, H.H. Wang, W. Xin, L. Li, M. K. Priydarshi, H. Yang, Z.B. Liu, J.G. Tian, Y.Y. Zhang, Y.F. Zhang, Z.F. Liu, Fast growth and broad applications of 25-inch uniform graphene glass, Adv. Mater. 29 (2017) 1603428.
[33] A.C. Ferrari, J.C. Meyer, V. Scardaci, C. Casiraghi, M. Lazzeri, F. Mauri, S. Piscanec, D. Jiang, K.S. Novoselov, S. Roth, A.K. Geim, Raman spectrum of graphene and graphene layers, Phys. Rev. Lett. 97 (2006) 187401.
[34] Q. Ye, J. Wang, Z.B. Liu, Z.C. Deng, X.T. Kong, F. Xing, X.D. Chen, W.Y. Zhou, C. P. Zhang, J.G. Tian, Polarization-dependent optical absorption of graphene under total internal reflection, Appl. Phys. Lett. 102 (2013) 021912.
[35] B. Xu, K.T. Ooi, C. Mavriplis, M.E. Zaghloul, Evaluation of viscous dissipation in liquid flow in microchannels, J. Micromech. Microeng. 13 (2002) 53.
[36] J.W. Weber, V.E. Calado, M.C.M. Van De Sanden, Optical constants of graphene measured by spectroscopic ellipsometry, Appl. Phys. Lett. 97 (2010) 091904.
[37] B. Hou, R. Xiang, T. Inoue, E. Einarsson, S. Chiashi, J. Shiomi, A. Miyoshi, S. Maruyama, Decomposition of ethanol and dimethyl ether during chemical vapor deposition synthesis of single-walled carbon nanotubes, Jpn. J. Appl. Phys. 50 (2011) 065101.
[38] L.D. Landau, E.M. Lifshitz, Fluid mechanics: landau and lifshitz: course of theoretical, Physics (2013).
[39] M.W. Sigrist, Laser generation of acoustic waves in liquids and gases, J. Appl. Phys. 60 (1986) R83–122.